Journal of Nuclear Materials 390–391 (2009) 232–237

Contents lists available at ScienceDirect

Journal of Nuclear Materials

journal homepage: www.elsevier.com/locate/jnucmat

Edge plasma physics/plasma–wall interactions during high density operation in LHD

A. Komori *, T. Morisaki, S. Masuzaki [1], M. Kobayashi, Y. Suzuki, R. Sakamoto, S. Morita, M.B. Chowdhuri, M. Goto, J. Miyazawa, I. Yamada, K. Narihara, N. Ohyabu, A. Sagara, H. Yamada, O. Motojima, The LHD experimental group

National Institute for Fusion Science, 322-6 Oroshi-cho, Toki 509-5292, Japan

ARTICLE INFO

PACS:
52.55.Hc

ABSTRACT

Superdense plasma with a highly peaked electron density profile was obtained in the reduced recycling discharge in the Large Helical Device (LHD). During the discharge, a core region with a density as high as $\sim 5 \times 10^{20}$ m^{-3} and a temperature of ~0.8 keV is maintained by an Internal Diffusion Barrier (IDB) with a steep density gradient. In spite of such a high density at the core region, no serious impurity accumulation has been observed. According to the numerical calculation with the EMC3–EIRENE code, downstream parallel flow in the ergodic region plays an important role to screen the influx of impurities with its strong friction force. The divertor flux distribution and global recycling properties do not change so much as against the change in the dense core plasma.

© 2009 Elsevier B.V. All rights reserved.

1. Introduction

The high density operation for the fusion device is attractive, since it provides the high fusion output, together with the reduction of the engineering demand. Many experiments to obtain high density plasma have been performed in many toroidal devices, i.e. tokamaks and helical devices. In tokamaks, the density is limited by the disruption or MARFE, which is the well-known Greenwald density limit [1]. On the other hand, in helical devices, it is limited by radiation collapse, i.e. determined by the heating power, as is well documented by the Sudo scaling [2]. Some confinement improvement modes with high density have been reported, e.g. the pellet enhanced performance (PEP) mode [3] achieved in JET tokamak, the high density H-mode (HDH) [4] in W7-AS stellarator.

In LHD heliotron [5], the superdense core mode (SDC) achieved with the formation of an Internal Diffusion Barrier (IDB) [6,7], was first discovered in the Local Island Divertor (LID) [8,9] configuration with a central fueled condition by the repetitive pellet injection. In this mode, a superdense plasma with the central density of $\sim 5 \times 10^{20}$ m^{-3} is maintained by the formation of an IDB with extremely high density gradient. Coupled with the relatively high electron temperature, the IDB–SDC modes exhibit the highest performance ($n_0 T_0 \tau_E = 4.4 \times 10^{19}$ m^{-3} keV s) obtained so far in LHD [6]. Recently it has been found that the IDB–SDC mode can also be obtained in the open Helical Divertor (HD) configuration, if only the wall pumping works effectively.

During the IDB–SDC discharge, the large magnetic axis shift called 'Shafranov shift' due to the high plasma pressure at the core region takes place, which causes the considerable modification of the magnetic field structure. In the edge region of LHD, there exists an intrinsic ergodic layer surrounding the nested flux surfaces, which affects the edge plasma behavior, and it is widely know that the ergodic layer is modified by the Shafranov shift. The thickness of the ergodic layer and the ergodicity itself generally increase with the increase of the shift. The plasma in the ergodic layer is the interface between the core plasma and the plasma facing components including the vessel wall, and some of the magnetic field lines actually connect to the divertor plates. Therefore the edge plasma in the ergodic layer plays an important role in the recycling of fueling and impurity particles released from the surface of the materials.

In this paper, the edge plasma properties and its effect on the plasma–wall interactions are discussed, together with the short review of the IDB–SDC mode so far obtained in the LHD experiment. After describing the experimental setup in Section 2, characteristics of the IDB–SDC mode are presented in Section 3. The divertor flux and recycling property during the IDB–SDC discharge is shown in Section 4, and the impurity behavior is in Section 5. Finally summary is presented in Section 6.

2. Experimental setup

The LHD is the superconducting heliotron device of which poloidal/toroidal period numbers are 2/10, and major and averaged

* Corresponding author.
E-mail addresses: komori@lhd.nifs.ac.jp (A. Komori), masuzaki@lhd.nifs.ac.jp (S. Masuzaki).
[1] Presenting author.

0022-3115/$ - see front matter © 2009 Elsevier B.V. All rights reserved.
doi:10.1016/j.jnucmat.2009.01.064

minor radii are 3.5–4.1 m and 0.6 m, respectively. The maximum toroidal magnetic field is 3.0 T. Three neutral beams (NBs) with the total heating power of ~10 MW are injected to heat and sustain the plasma. Repetitive pellet injectors are utilized to realize the central fueling. The electron density n_e and temperature T_e profiles are measured with the Thomson scattering system, and the line averaged density with a far infrared interferometer. The line emissions from impurities are measured with spectroscopic method.

The LHD has two different divertor configurations, i.e. LID and HD. The LID is a kind of the island divertor which utilizes an externally induced $m/n = 1/1$ island located in the edge region, where m and n are poloidal and toroidal mode numbers, respectively. A schematic of the LID is presented in Fig. 1. Particles diffusing out from the core region flow along the separatrix or periphery of the island. Going around the island, they reach the outer separatrix of the island where the LID head is placed, and strike its backside on which they are neutralized. Particles recycled there are pumped out efficiently by the strong pumping system with a baffle integrated into the closed divertor configuration. On the other hand the HD is an intrinsic divertor for the heliotron configuration, which is similar to the tokamak double null divertor with four divertor legs. In the HD configuration there is a thick ergodic layer outside the separatrix, which does not exist in the LID configuration.

For the three-dimensional equilibrium calculation, the HINT2 code [10] is utilized, which has recently been developed on the basis of the HINT code. With HINT2, one can deal with the calculation volume where magnetic field lines are not always perfectly closed, i.e. the ergodic layer. In order to investigate the impurity transport properties in the ergodic layer of LHD, the 3D numerical edge transport code [11], EMC3 [12]–EIRENE [13], is applied to the Helical Divertor configuration. The realistic three-dimensional geometry of magnetic field line structure of the ergodic region as well as vessel wall/divertor plates are precisely treated by the code.

3. IDB–SDC discharges

As mentioned in Section 1, the IDB–SDC mode was first discovered in the LID configuration with strong edge pumping capability. During the experiment, as an optimization of the fueling, a series of pellets were injected without gas puffing. These pellets penetrated around the magnetic axis, hence brought about the central deposition of the fueling particles. After several pellets of $N \sim (2–3) \times 10^{21}$ atoms/pellet were injected to the NB heated plasma, the density profile presented a peaked shape. Subsequent pellet injection continuously raised n_{e0} until the final pellet was injected. Since the NBs kept on heating the plasma, electron temperature T_e at the central region started to rise, according to the decrease of the electron density. Consequently the plasma stored energy W_p had its maximum a few hundred ms after the final pellet was injected.

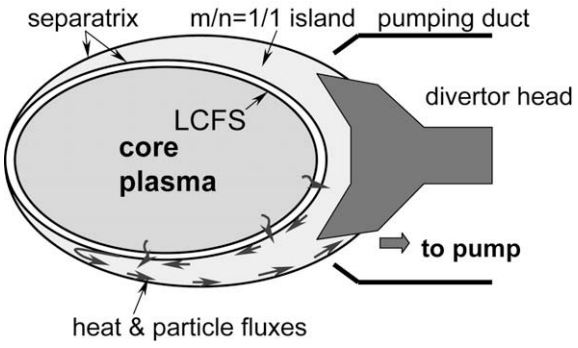

Fig. 1. A schematic of LID.

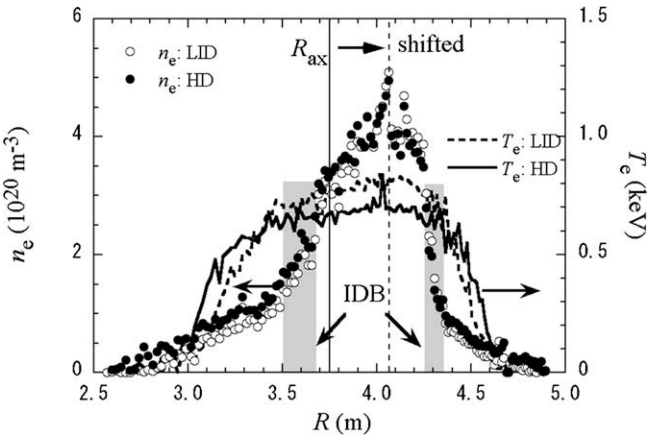

Fig. 2. Typical profiles of electron density n_e (open circles) and electron temperature T_e (dashed line) in the LID configuration when the plasma stored energy is the maximum during the IDB–SDC discharge. Those in the HD configuration are also depicted with closed circles and a solid line.

In Fig. 2, typical radial electron density and temperature profiles in the LID configuration at the time when W_p reached its maximum are depicted with open circles and a dashed line, respectively. It can be seen that a core region with electron density $\sim 5 \times 10^{20}$ m^{-3} and temperature ~0.85 keV is maintained by the IDB, which provides the highest fusion plasma performance, $n_0 T_0 \tau_E \sim 4.4 \times 10^{19}$ keV m^{-3} s [6], achieved so far on LHD. From the Ar Doppler-broadening at the plasma center, it has been known that central ion temperature $T_i(0)$ is almost equal to $T_e(0)$ measured with the Thomson scattering system. The radial width of the IDB is about 0.1 (outboard side of the torus) – 0.4 (inboard side) m. Due to the high central plasma pressure more than 1 atm ($\beta_0 \sim 4.4\%$), a large Shafranov shift about a half of the minor radius is observed. In the figure the original magnetic axis position and shifted one are depicted with thin solid line and dashed line, respectively.

To achieve the IDB–SDC mode the strong pumping and the central fueling are essential. In the recent experiments it has been

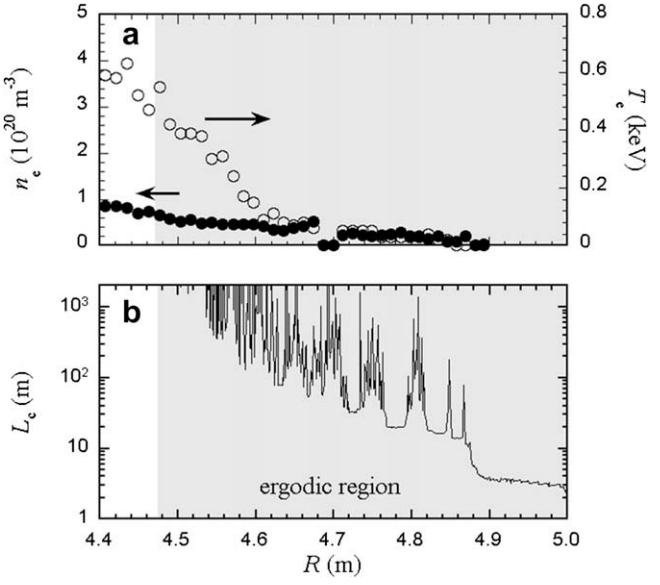

Fig. 3. (a) Edge density and temperature profiles obtained in the IDB–SDC discharge in the HD configuration and (b) connection length L_c profile of the magnetic field lines. Hatched region indicates the ergodic layer.

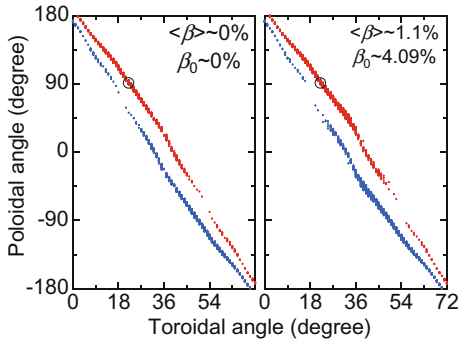

Fig. 4. Toroidal and poloidal divertor flux distribution calculated with the HINT2 code coupled with the diffusion effect. The left hand side is for the vacuum or low beta discharge and the right hand side for the IDB–SDC discharge. Position of the probe array embedded in the divertor plate is shown with small circle.

found that exhaustive wall conditioning enables the IDB–SDC discharge even in the open HD configuration, instead of the strong pumping with LID. The established profiles in the HD configuration (closed circles and solid line in Fig. 2) are almost the same as in the LID configuration, except that the central temperature in the HD configuration is slightly low. This is a very promising result, from the engineering point of view, since the wetted area on the target plates in the HD configuration is much larger than that in LID. The heat load to the divertor plates can be removed much safely in the HD configuration.

As mentioned above, the edge plasma properties in the HD configuration are similar to those in the LID configuration. Fig. 3 shows edge density and temperature profiles obtained in the IDB–SDC discharge in the HD configuration, together with the connection

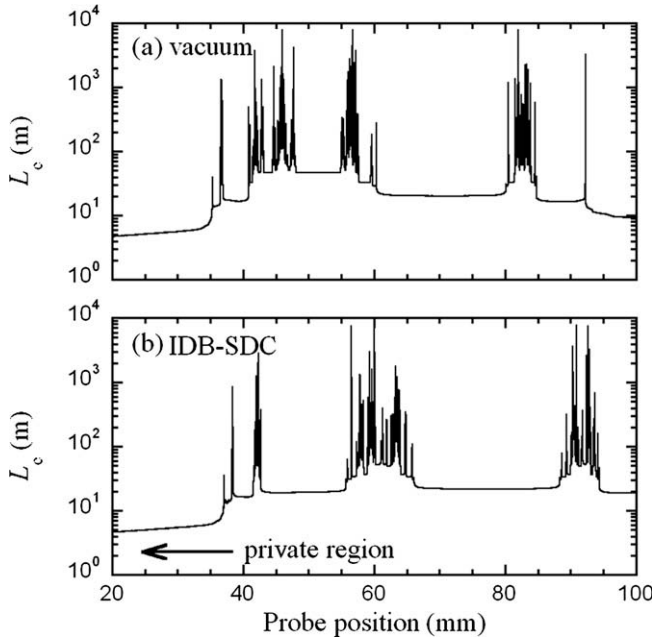

Fig. 6. Connection length profiles of the magnetic field lines (L_c) on divertor plate for (a) vacuum condition and (b) IDB–SDC phase calculated with HINT2 code.

length profile L_c of the magnetic field lines, calculated with the HINT2 code using the experimentally obtained pressure data. The oscillation in L_c reflects the ergodic property of the magnetic field structure. However, the actual ergodic layer is wider than the L_c-oscillating region because, in the ergodic layer, the magnetic field

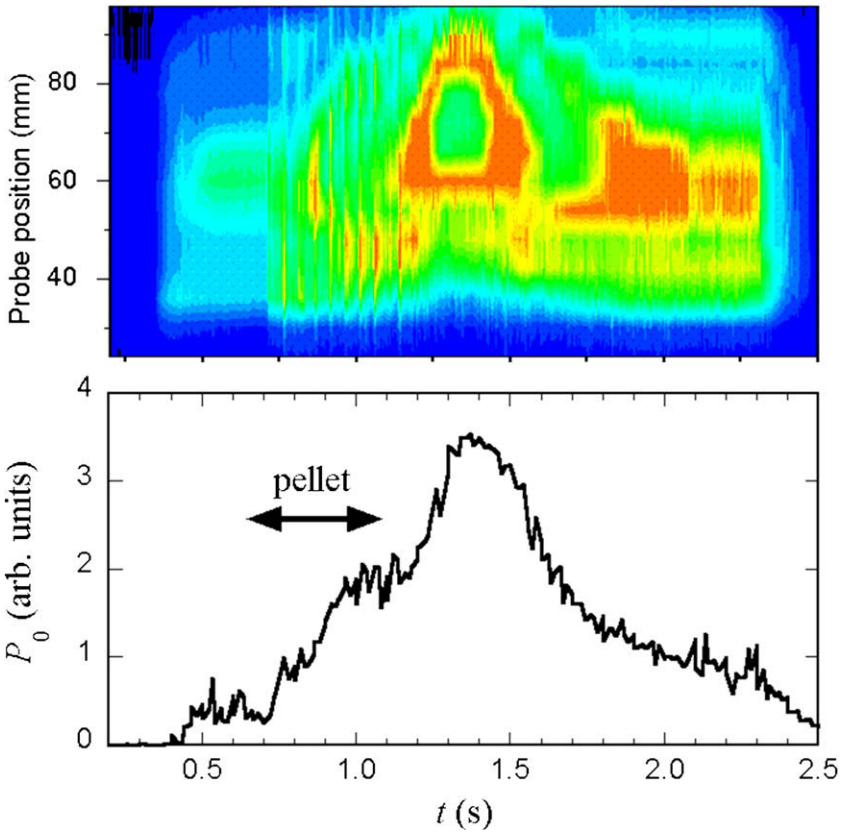

Fig. 5. Time evolutions of the ion saturation current (I_{sat}) profiles on a divertor plate during the IDB–SDC discharge, together with the central plasma pressure.

lines with quite long L_c over the range of Fig. 3(b) exist, which make complicated excursions with radial deviation. It is found from the Fig. 3 that T_e rises from the far edge region in the ergodic layer with steep gradient, suggesting the quite small energy transport property there. On the other hand n_e profile is relatively flat. This result observed in the IDB–SDC discharge is qualitatively inconsistent with conventional transport theory for ergodic region [14]. Similar observation is reported from the ELM (edge localized mode) control experiment applying the resonant magnetic perturbations (RMPs) in DIII-D [15]. The mechanism for the energy and the particle transport in the ergodic layer may be common between tokamaks and helical devices. Further investigation should be carried out in both configurations to clarify the underlying physics.

4. Divertor flux during the IDB–SDC discharge

The edge or divertor magnetic field has complicated three-dimensional structure in LHD, thus the toroidal/poloidal distribution of the divertor flux or its profile on a divertor plate reflects the edge magnetic field structure [16]. In the IDB discharge, the central beta is large enough to modify the edge magnetic field structure. Fig. 4 shows the divertor flux distribution on the toroidal-poloidal plane where target plates locate, by using a field line tracing code coupled with the three-dimensional equilibrium code called HINT2. The diffusion effect was taken into account in the calculation as a random walk process. In the equilibrium calculation the central beta was set to be 4.1% and the diffusion coefficient to be ~1.0 m^2/s. It is found that the toroidal and poloidal distribution of the divertor flux is not changed so much between low beta and high beta (IDB–SDC) discharges. On the other hand, the flux distribution on each divertor plate changes when IDB–SDC is established. Fig. 5 shows the time evolutions of the ion saturation current (I_{sat}) profiles on a divertor plate measured with the Langmuir probe array during the IDB–SDC discharge, together with the time evolution of the central plasma pressure. The position of the divertor plate in which the probe array is embedded is shown in Fig. 4 with small circles. After the termination of the pellet injection at t = 1.05 s, the IDB is formed and I_{sat} profile largely changes from t = 1.1 s to 1.6 s with the increase of the central plasma pressure. At t = 1.25 s two peaks appear at ~60 mm and ~90 mm. Fig. 6 shows the connection length profiles of the magnetic field lines (L_c) on the divertor plate for (a) vacuum condition and (b) IDB–SDC phase. For the field line tracing, the equilibrium data calculated with the HINT2 code was also utilized. In both cases, L_c profiles have several peaks. Long field lines with L_c of more than several hundred meters are connecting divertor plates with the region near the last closed flux surface (LCFS), which can be the main streams of parallel transport. Therefore peaks in the heat and particle flux profiles are related to those in L_c profile. Comparing Fig. 5 with Fig. 6, it can be seen that peak positions of I_{sat} and L_c roughly coincide with each other. This suggests that the modification of the

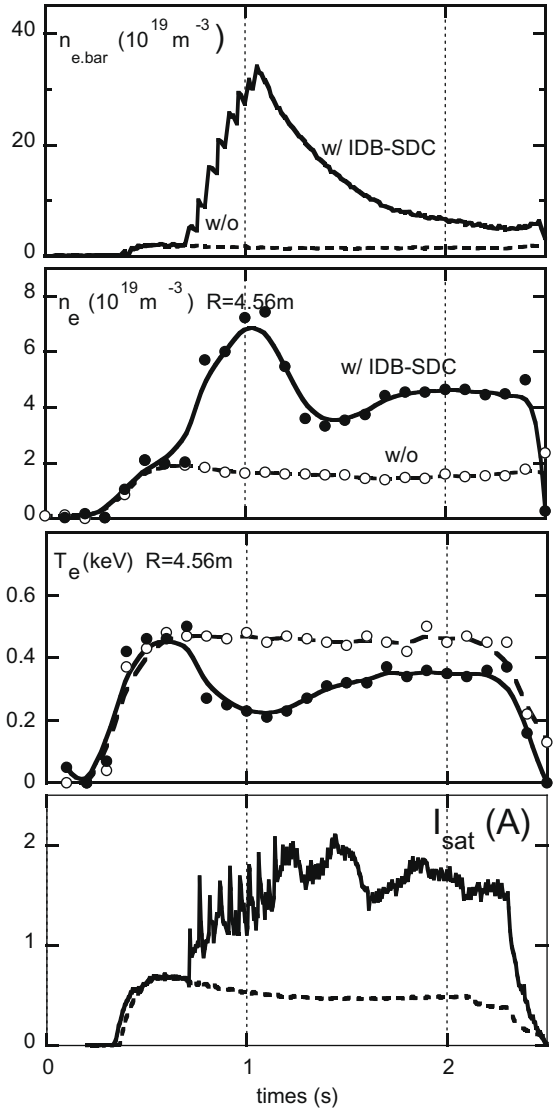

Fig. 7. Time evolution of line averaged density, edge density, edge temperature and summation of I_{sat} of the Langmuir probe array for the discharge with and without the IDB–SDC.

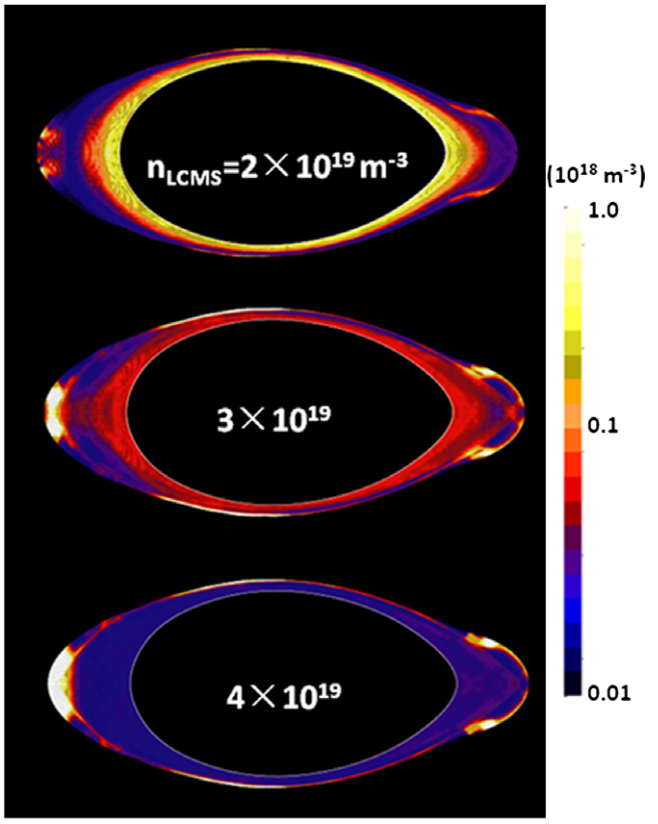

Fig. 8. Carbon density profiles obtained by EMC3–EIRENE for different background densities, n_{LCFS} = 2 × 10^{19}, 3 × 10^{19}, 4 × 10^{19} m^{-3}. LCFS is computational boundary.

edge magnetic field structure affects the particle flux profile on divertor plates.

Fig. 7 shows the time evolution of line averaged density, edge density, edge temperature and summation of I_{sat} of the Langmuir probe array, for the discharges with and without the IDB–SDC. During the IDB–SDC mode (t = 1.2–1.6 s), the line averaged density is $\sim$1–2 $\times$ 10^{20} m^{-3} which is 5–10 times higher than that in the discharge without SDC. On the other hand, the edge density and I_{sat} during the IDB–SDC mode is only about 2–3 times higher than that in the discharge without SDC. Furthermore the difference in the edge electron temperature is less than twice. It can be seen from these experimental results that the edge plasma does not change so much during SDC mode, in spite of the drastic change in the core region.

5. Impurity behavior

Impurity transport analysis in the ergodic layer of LHD has been conducted using 3D edge transport code [11], EMC3 [12]–EIRENE [13]. Fig. 8 shows carbon density profiles in horizontally elongated cross section for different background plasma density obtained by the 3D modelling. At low density, $\sim$2 $\times$ 10^{19} m^{-3}, the carbon is accumulated around LCFS, which is the boundary of the computational domain. The edge plasma parameters obtained by the 3D modelling are plotted in Fig. 9, together with the ratio between friction force and ion thermal force. At lower density, the ion thermal force caused by parallel temperature gradient, $2.6Z^2\partial T_i/\partial s$, dominates over friction force (i.e. friction force/thermal force $\ll$1), where Z is charge number of impurity and s coordinate along magnetic flux tube, the direction of which is upstream due to the temperature drop toward divertor plate. At higher density, on the other hand, the friction force, $m_z(V_i - V_z)/\tau_s$, starts to dominates over thermal force due to increasing collisionality, where m_z, V_i, V_z, τ_s are mass of impurity, background parallel plasma flow, impurity parallel flow and collision time between impurity and background plasma, respectively [11].

The friction force exerted by the background plasma flow, directs toward divertor plate. As a consequence, the impurity is effectively screened in the very edge of ergodic layer at the higher density, as shown in Fig. 8. The collisionality of the each density is estimated as $\nu^*\varepsilon^{3/2} = 0.13$ (n_{LCFS} = 2 $\times$ 10^{19} m^{-3}) and 0.58 (n_{LCFS} = 4 $\times$ 10^{19} m^{-3}), normalized by helical ripple ε (=0.27 at last closed flux surface) to the power of 3/2. Here the collisionality is defined as

$$\nu^* = \frac{\nu_{zi} R_0}{\nu_{th}\varepsilon^{3/2}\iota},$$

where ν_{zi}, R_0, ν_{th}, ι are collision frequency between impurity (carbon, Z = 6) and background plasma ion, major radius, thermal speed of background ion, rotational transform, respectively.

When the screening occurs in the ergodic layer, the carbon ions with higher charge states decrease compared to ones with lower charge states. Since we have found that the temperature profile keeps its slope (shape) unchanged during the density scan, the radiation intensity (normalized by background plasma density) is considered to reflect the behavior of impurity number density rather than the temperature effect. Fig. 9(a) and (b) shows carbon radiation intensity of CIV (1548 Å) and CV (40.27 Å) obtained by VUV monochromators and CV with EUV spectrometer, respec-

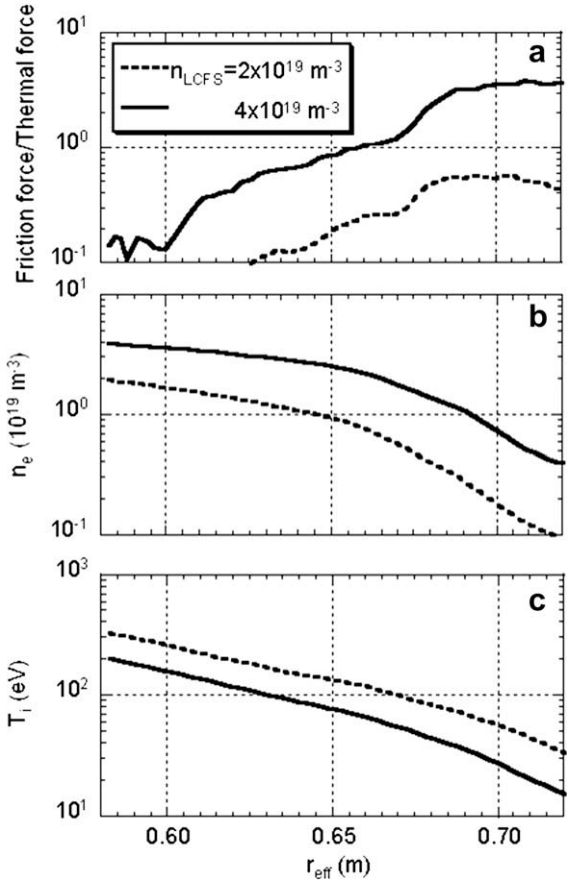

Fig. 9. (a) Radial profiles of ratio of friction force to ion thermal force, (b) background plasma density, (c) background ion temperature, for low (n_{LCFS} = 2 $\times$ 10^{19} m^{-3}) and high (n_{LCFS} = 4 $\times$ 10^{19} m^{-3}) density cases. The profile is averaged over poloidal and toroidal direction. r_{eff} is defined by a constant volume in cylindrical approximation enclosed by each radial computational mesh.

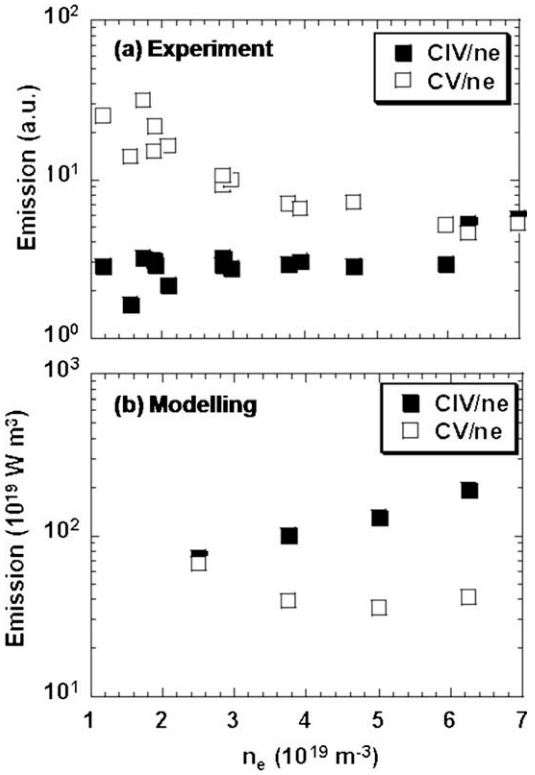

Fig. 10. (a) CIV and CV emission obtained by VUV monochromators, and CV with EUV spectrometer, respectively, as a function of density. (b) CIV and CV emission obtained by EMC3–EIRENE, as a function of density. The emission is normalized by background plasma density.

tively, and by the EMC3–EIRENE, as a function of density. The ionization potentials of the two charge states are largely different, CIV: 65 eV and CV: 392 eV. The code results are obtained by integrating carbon emission inside the line of sight of spectroscopy. Since the measurement system is not absolutely calibrated, we can not compare the absolute tendency at the moment. The density dependence is, however, in qualitative agreement with each other, i.e. increase of CIV and decrease of CV, respectively. It should be noted, that since the ratio of the thermal force and friction force becomes charge independent, the screening model applies also for high-Z impurity such as Fe another intrinsic impurity in LHD. The mechanism of the screening in the ergodic layer is an important feature of LHD and might be able to explain the low Z_{eff} measured during extremely high density operation like IDB plasma (see Fig. 10).

6. Summary and discussions

The superdense core (SDC) mode with central density $\sim 5 \times 10^{20}\,m^{-3}$ was maintained for $\sim$1 s by the formation of an Internal Diffusion Barrier (IDB) in LHD. The central electron temperature in IDB–SDC plasmas is relatively high as $\sim$0.85 keV. It is considered that low density in the outer region helps to raise the edge temperature gradient there and hence the core temperature. In order to obtain the IDB–SDC mode, the pellet injection (central fueling) and the strong edge pumping (low edge recycling) are essential. In the ergodic region n_e profile is relatively flat, on the other hand, T_e profile has a steep gradient, which cannot be explained with the conventional transport theory for ergodic region [14]. In spite of the strong edge modification by the large Shafranov shift in the IDB–SDC discharge, the PSI-related phenomena is not so affected by the core plasma parameters, i.e. divertor flux and its distribution are not so different from those of ordinary discharges. Impurities are well shielded in the ergodic region by the friction force between plasma flow from the inner region. Experimental results encourage us to study the new approach to the reactor plasma with IDB–SDC regime.

Acknowledgements

Authors would like to thank all members of device engineering group for their support and operation of the machine. This work is funded by NIFS07ULPP506 and the Grant-Aid for Scientific Research from MEXT of the Japanese government.

References

[1] M. Greenwald et al., Nucl. Fusion 28 (1988) 2199.
[2] S. Sudo et al., Nucl. Fusion 30 (1990) 11.
[3] M. Hugon, B.Ph. van Milligen, P. Smeulders, et al., Nucl. Fusion 32 (1992) 33.
[4] K. McCormick, P. Grigull, R. Burhenn, et al., Phys. Rev. Lett. 89 (2002) 015001.
[5] O. Motojima, H. Yamada, A. Komori, et al., Phys. Plasmas 6 (1999) 1843.
[6] N. Ohyabu, T. Morisaki, S. Masuzaki, et al., Phys. Rev. Lett. 97 (2006) 055002.
[7] T. Morisaki, N. Ohyabu, S. Masuzaki, et al., Phys. Plasmas 14 (2007) 056113.
[8] A. Komori, T. Morisaki, S. Masuzaki, et al., Fusion Sci. Technol. 46 (2004) 167.
[9] T. Morisaki, S. Masuzaki, A. Komori, et al., J. Nucl. Mater. 337–339 (2005) 154.
[10] Y. Suzuki, N. Nakajima, K. Watanabe, et al., Nucl. Fusion 46 (2006) L19.
[11] M. Kobayashi et al., Contrib. Plasma Phys. 48 (2008) 255.
[12] Y. Feng et al., Contrib. Plasma Phys. 44 (2004) 57.
[13] D. Reiter et al., Fusion Sci. Technol. 47 (2005) 172.
[14] A.B. Rechester, M.N. Rosenbluth, Phys. Rev. Lett. 40 (1978) 38.
[15] T.E. Evans, R.A. Moyer, K.H. Burrell, et al., Nat. Phys. (21) (2006), doi:10.1038/nphys312.
[16] S. Masuzaki, T. Morisaki, N. Ohyabu, et al., Nucl. Fusion 42 (2002) 750.